African Journal of Agricultural Research Vol. 6(12), pp. 2920-2930, 18 June, 2011
Available online at http://www.academicjournals.org/AJAR
DOI: 10.5897/AJAR10.916
ISSN 1991-637X ©2011 Academic Journals

Full Length Research Paper

Filling gaps in vegetation index measurements for crop growth monitoring

Yaohuan Huang, Dong Jiang*, Dafang Zhuang, Hongyan Ren and Zhijun Yao

Data Center for Resources and Environmental Sciences, State Key Laboratory of Resources and Environmental Information System, Institute of Geographical Sciences and Natural Resources Research, Chinese Academy of Sciences, 11A Datun Road, Chaoyang District, Beijing 100101, China.

Accepted 1May, 2011

Vegetation index (VI) derived from satellite data is a key indicator for researches on crop type identification, growth monitoring and yield forecasting. However, due to the influences of the disturbance factors including the cloud contamination, atmospheric variability and bi-directional effects, the time series VI data are always with significant fluctuations. Such limitations greatly constrain the further application of time-series VI data. How to reconstruct high-quality time-series VI data has become a challenge especially for regional study. In this study, an operational method based on Savitzky–Golay filter was adopted for reconstructing MODIS Enhanced Vegetation Index (EVI) data from 2000 to 2008 in the Haihe River Basin in North China. The reconstructed EVI time-series dataset was analyzed together with land-use map and evapotranspiration data. It is found that this method can significantly reduce the containments of clouds and some other abnormal noises, and can greatly improve the quality of EVI time-series dataset both in space and time. It is also noted that this approach shows limitations for some small built-up lands dotted in vegetation land. We discuss the possible reasons in further research.

Key words: Vegetation index, crop monitoring, Savitzky–Golay filter.

INTRODUCTION

Vegetation of land surface is always the first layer of information that remote sensing gained and is one of the important ways to study crop growth situation and yield forecasting (Zhao et al., 2003). Many kinds of Vegetation index (VI) have been developed to show the information of vegetation. Most of these attempts focused on the differences of the absorptive and reflective electromagnetic spectrum properties between the visible (VIS) and near-infrared (NIR) portions, for example, normalized difference vegetation index (NDVI), SAVI, TSAVI, MSAVI, DVI, GVI, PVI, EVI, etc. (Zhao, 2003). It has been found that time-series VIs derived from NOAA/AVHRR, SPOT/VEGETATION, TERRA, or AQUA/MODIS are valid for detecting long term development of vegetation, plants phenology, evapotranspiration, drought, corn yield, land-use/cover changes, and terrestrial ecosystems at different spatial and temporal resolutions globally (Justice et al., 1985; Toshihiro et al., 2005; Unganai et al., 1998; Running et al., 1988; Tucker et al., 1985; Chen et al., 2004). Theoretically, a generalized VI temporal profile is continuous and smooth because vegetation canopy changes are subtle with respect to time (Ma et al., 2006). However, there are always some disturbances which make time-series VI data fluctuate with remarkable rises and falls. The possible causes are cloud contamination, atmospheric variability and bi-directional effects. Besides, some VI data products have a lot of no-data pixels because of hardware or human factors (Viovy et al., 1992). For instance, the MODIS/Terra Vegetation Indices 16 day L3 Global 1 *km* SIN Grid (MDO13A2) is a 16 day maximum value composite (MVC) product. It has its own QA sub-datasets to indicate the reliability and quality of the pixel values. The values of pixels with poor quality are artificial and will bring errors to the following researches. More and more researchers realize that the precision of

*Corresponding author. E-mail: jiangd@igsnrr.ac.cn Tel: +86-10-64889433. Fax: +86- 10-64855049.

the final results of crop growth models not only depends on the models they choose but also the accuracy of the input data. A series of approaches have been developed to reduce the errors of the noises in VI data and to reconstruct high quality time-series data sets, for example, the maximum value composite (MVC) (Huete et al., 1999), the Mean-value iteration filter (MVI) (Ma et al., 2006), the best index slope extraction (BISE) method (Viovy et al., 1992; Lovell et al., 2001), Fourier analysis (Cihlar, 1996; Cihlar et al., 1997), the weighted least-squares approach (Swets et al., 1999), the polynomial least squares operation (PoLeS) method (Jose et al., 2002), geo-statistics (Chappell et al., 2001), and asymmetric Gaussian function fitting (Jonsson et al., 2002).

Although the aforementioned methods have been employed in related researches and received good results, they suffer from their own drawbacks which limit their use (Chen et al., 2004; Ma et al., 2006; Jonsson et al., 2002). For example, the algorithm of MVC and MVI ignores the remarkable anisotropy of reflectivity and VI, which may conceal details of vegetation with too large interval and lead to the result of reconstructed VI data from MVC and MVI with lot of noises remaining. The BISE and other threshold-based methods may make the extracted temporal information unreliable (Running et al., 1988). The Fourier analysis algorithm is sensitive to spurious peaks of the VI trend line, so it may depart from the truth a lot (Chen et al., 2004; Jonsson et al., 2002). A simple algorithm based on Savitzky–Golay filter was explored by Chen for processing SPOT/VEGETATION data in 2004 (Chen et al., 2004). This method is thought to be more efficient than other methods mentioned previously: (1) there are no restrictions on the scaling of the VI and the specific sensor, (2) for irregular or asymmetric VI time series data, it can made smaller displacement away from the original values than some other methods such as Fourier-based fitting methods, it can get almost identical result as the complex methods such as BISE algorithm but easy to implement without the difficulty of finding an optimal threshold, and (4) it can be applied to VI data sets with different intervals such as daily data, 10 day, or monthly MVCs. Since the early 2000s, MODIS EVI products have been widely used for their spatial and temporal advantages. In our study, Chen's method was applied to reduce the residual contaminations of MODIS EVI data. The 1 *km* 16 day composite images (from end-December of 2000 to early-January of 2008) which cover the whole Haihe River Basin in North China were obtained from NASA ftp sites and processed. Our study focuses on how to select and validate suitable reconstructing approaches for the time-series EVI data at regional scale. The reconstructed EVI time-series datasets were analyzed together with different land-use types, which were extracted from the China and Brazil Earth Resource Satellite (CBERS) images and evapotranspiration data. Both the advantages and limitations of the algorithm were also discussed.

STUDY AREA

The study area, Haihe River Basin, lies in North China from 34°09′N to 43°11′N, 111°21′E to 120°43′E (Figure 1a). It consists of eight provinces, including Beijing, Tianjin, most areas of Hebei, and some parts of Shandong, Henan, Shanxi, Inner Mongolia and Liaoning. The total area of Haihe River Basin is 318,000 km^2 with approximate 40% plain and 60% mountainous areas. Figure 1b shows the elevation of the basin, which decreases from west to east and ranges from 2983 to 1 m. The basin covers various land-use types and vegetation-covers, including cropland, built-up land, forest, grass land etc. According to relevant statistics, in 2004, the vegetation land accounts for 94% out of Haihe River Basin and only less than 6% area are built-up land. It's one of the major grain producing areas of China and the three main crop types in Haihe River Basin are wheat, corn and cotton.

METHODOLOGY

General introduction of Savitzky–Golay filter

The Savitzky-Golay filter, also known as the least squares or digital smoothing polynomial (DISPO), was developed by Savitzky and Golay (1964). The filter, which can be used to smooth a noisy signal, is defined as a weighted moving average with weights given as a polynomial of a certain degree. When applied to a signal, the coefficients returned from the Savitzky-Golay smoothing filter perform a polynomial least-squares fit within the filter window. The polynomial is designed to preserve higher moments within the data and to reduce the bias introduced by the filter. The filter can use any number of points for this weighted average, and it works especially well when the typical peaks of the signal are narrow. The heights and widths of the curves are generally preserved. Based on the characters of the Savitzky-Golay, it can be used to reconstructing the VI data. Chen has applied it to smoothing the 10 day MVC SPOT VEGETATION time-series data (Chen et al., 2004), the general equation is described as following:

$$Y_j^* = \frac{\sum_{i=-m}^{m} C_i Y_{j+1}}{N} \quad (1)$$

where Y is the original EVI value, Y^* is the resultant EVI value, C_i is the coefficient for the ith value of the filter, and N is the number of convoluting integers and is equal to the smoothing window size ($2m$+1). The index j is the running index of the original ordinate data table.

We implemented the process of Savitzky-Golay filter on the platform of the commercial software of interactive data language (IDL). There are two important parameters in the Savitzky-Golay smoothing filter generation function of SAVGOL which are m and d. The parameter m is an integer specifying the number of data points to the left or right of each point to be included in the filter, and is

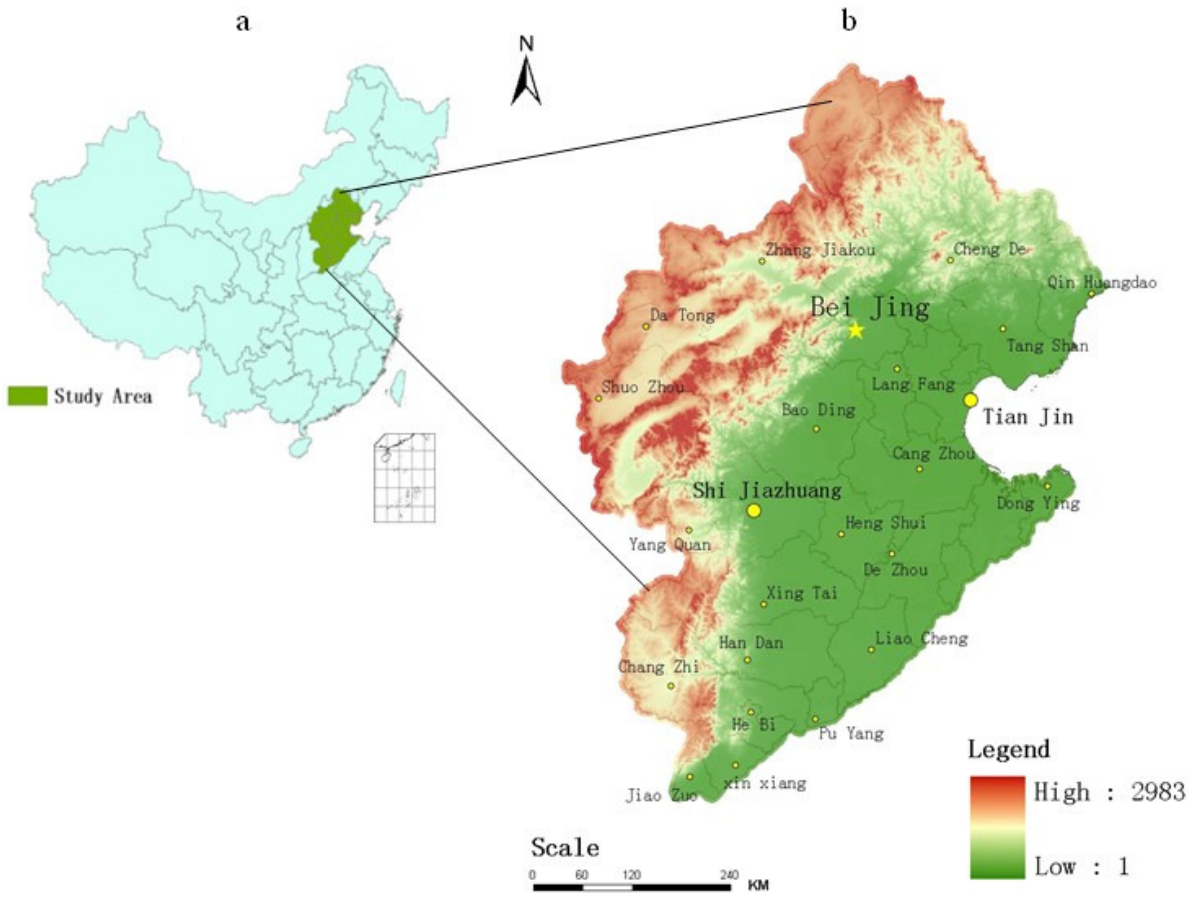

Figure 1. (a) Location of the study area, (b) Haihe River Basin.

determined as half-width of the smoothing window. The parameter *d* is to describe the degree of smoothing polynomial. Typical values of *d* vary from 2 to 4. Lower values for *d* will produce smoother results but may introduce bias. A higher *d* helps reduce the filter bias, but it may "over fit" the data and lead to a noisier result. Chen et al. (2004) determined the value of *d* and *m* through a series of experiments based on 438 testing pixels. He and his colleagues proposed that the (*d, m*) combination of (6, 4) was the optimized. In our study, we also respectively set the *d* and *m* as 6 and 4.

Reconstruction algorithm

The application of Savitzky-Golay filter to the reconstruction of the high-quality MODIS EVI time-series data is based on two hypotheses proposed by Chen (2007): (1) the EVI data from a satellite sensor is primarily related to vegetation changes. As such, an EVI time-series follows annual cycle of growth and decline; and that (2) clouds and poor atmospheric conditions usually depress EVI values, requiring that sudden drops in EVI, which are not compatible with the gradual process of vegetation change, be regarded as noise and removed (Chen et al., 2004). The flowchart of EVI reconstruction process is illustrated in Figure 2.

Preprocessing of MODIS EVI data

We downloaded the MOD13A2 dataset from NASA EOS data Gateway (EDG) (http://modis.gsfc.nasa.gov/index.php). The original MODIS EVI data (MOD13A2) used in this study is one of the MODIS land products. There are 12 sub-layers stored in Hierarchical Data Format (HDF) for MOD13A2 data. Three EVI related layers inside MOD13A2 dataset are 1 *km* 16 days EVI, 1 *km* 16 days VI Quality and 1 *km* 16 days pixel reliability. All of the three layers are with the projection of Sinusoidal (SIN). We firstly composed the original data and re-projected them with the help of MODIS reprojection tool (MRT). After that, we calibrated the value of EVI layer to real value and combined quality layers to a quality assurance (QA) dataset. The calibrate equation involved in this process is defined as:

$$EVI = \text{scale} \times D + \text{offset} \quad (2)$$

Where *EVI* is the real value. Scale and offset are respectively valued as 0.0001 and 0. *D* is the value in the original EVI layer. Additionally, the filling value of -3000 is removed.

The MOD13A2 v005 provides two QA layers which can be used to identify poor quality pixels. We firstly classify the pixels into 3 categories (that is, useful, uncertain and bad) according to the pixel reliability of the layer of 1 *km* 16 days.

Regarding to those pixels that are hard to be classified, we used another QA information layer, the 1 *km* 16 days VI quality layer, to further examine them. We converted the values of the 1 *km* 16 days VI Quality layer to 15 bits binary words which represent 9 kinds of QA significances. Considering the following application of the

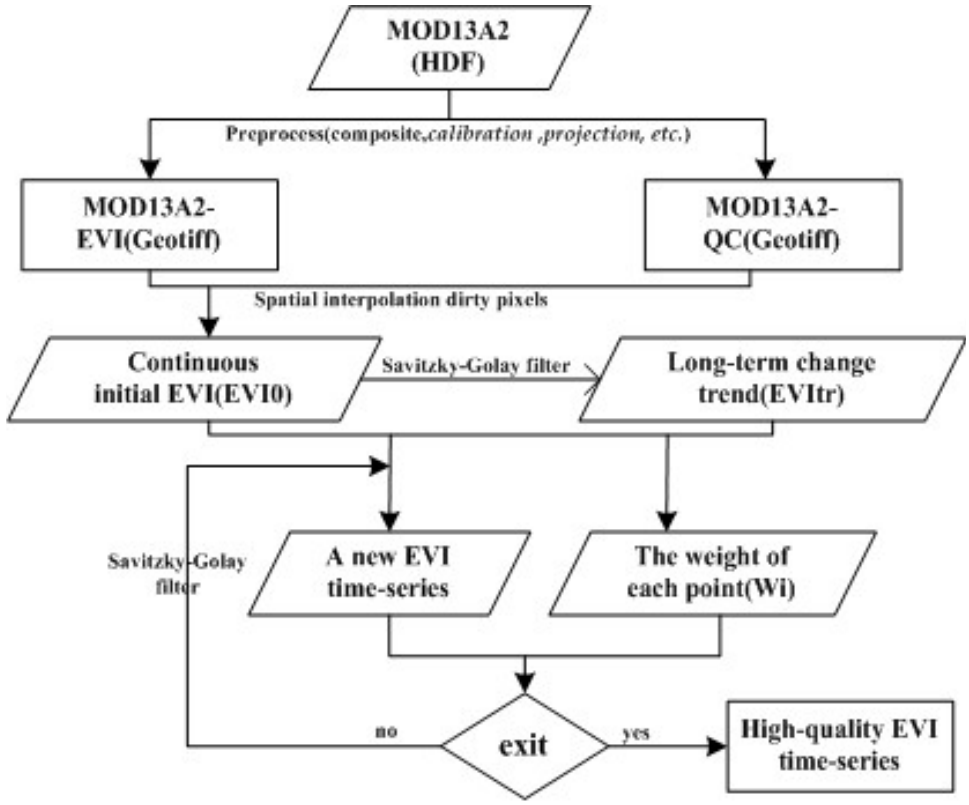

Figure 2. Flowchart of the reconstruction process of MOD13A2-EVI based on Savitzky-Golay filter in Haihe River Basin.

reconstructed EVI, we chose the bit 0 to bit 1 which represent VI Quality (MODLAND) and bit 2 to bit 5 which represent VI usefulness to estimate the quality of related uncertain pixels. In this manner, we can estimate the quality of related uncertain pixels.

Considering the real growth life of vegetation, pixels whose EVI values increased more than 0.3 during 16 days are identified as bad pixels. This may be caused by bi-directional effects. Therefore, we build a new QA data set where the EVI data is described as either good or bad. The bad pixels are named poor quality pixels. Figure 3 shows the QA distribution of a MOD13A2-EVI image from 26 June to 11 July 2005. As shown in Figure 3a, three kinds of quality pixies exist after first classification according to the layer of 1 *km* 16 days pixel reliability. There are 149,271 uncertain pixels, accounting to nearly 47% of the total 318075 pixels. Figure 3b shows the final QA result of the image after being processed by the method mentioned previously. We found 32,903 poor quality pixels exist, which means that about 10% of the pixels are incongruous with others. This finding further supports our point of view that directly using the original data will cause errors in following research.

Spatial interpolation of poor quality pixels

The Savitzky-Golay filter process requires continuous data, while the MOD13A2-EVI is not continuous as it contains poor quality pixels (for example, cloudy, not being processed). We have to interpolate the poor quality pixels of EVI data, which relies on the QA dataset generated in preprocessing of MODIS EVI data in spatial, to produce a continuous dataset. Firstly, for a given pixel with poor quality, we searched eight nearest pixels with good QA and recorded the value of those eight pixels and their distance (d_i) to give the poor quality pixel. Figure 4 describes the eight directions searching.

After that, the inverse distance weighted interpolation method (IDW) is applied to compute the values of the given pixel. According to the definition of IDW, we can define EVI as:

$$EVI = \sum_{i=1}^{8} \lambda_i EVI_i, \qquad \lambda_i = \frac{d_i^{-1}}{\sum_{1}^{8} d_i^{-1}} \tag{3}$$

Where *EVI* is EVI value of poor quality pixel after interpolation and *EVIi* is the EVI value of a good pixel. The continuous initial EVI time-series is recorded as *EVI0*.

To the poor quality pixels, IDW will smooth the image in space, while latter time-series process will offset this effect in most cases. However, if most part of an image is poor-qualified pixels, which may be caused by data transmission errors, the previous interpolation method shows some limitations, we will study them later. Taking the thirteenth image as an example, because more than 70% pixels in Haihe River Basin are with the filling value of -3000, the interpolation process will introduce error for lack of value.

Generation of high-quality EVI time-series with the Savitzky-Golay filter

We carried out time-series analysis for each pixel in the 163 images in seven years. For each pixel, we firstly generated a time-series

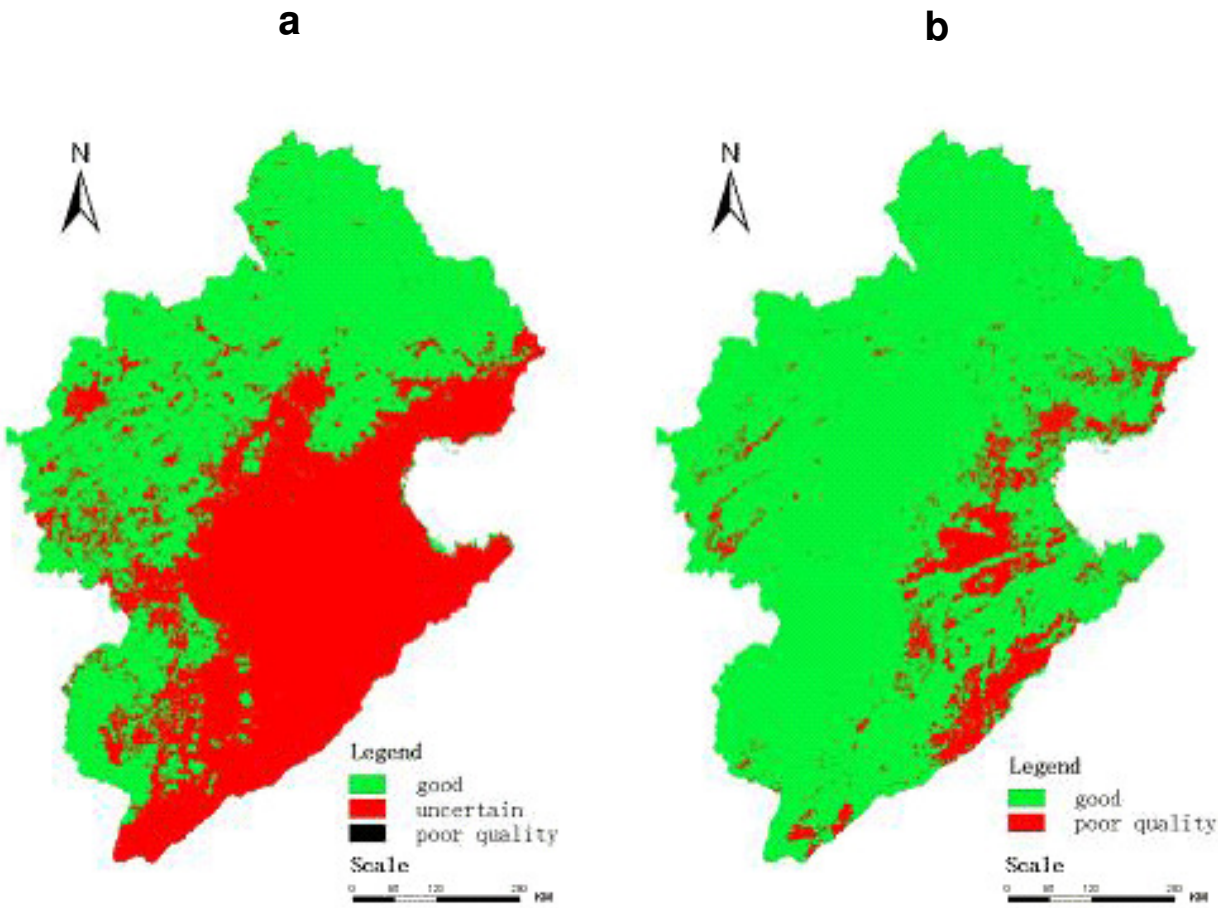

Figure 3. (a) QA distribution of a MODIS EVI image from 26 June to 11 July 2005 and (b) final QA.

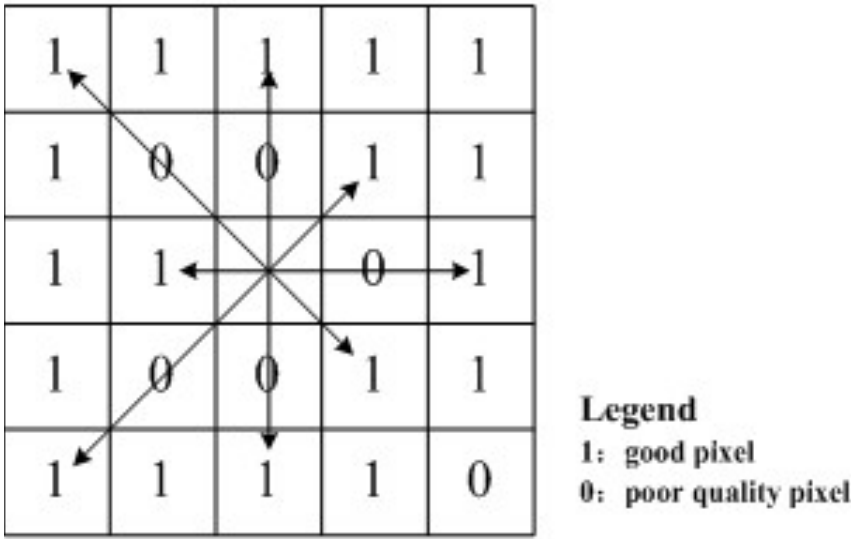

Figure 4. Eight directions searching.

curve on the basis of the *EVI0* data, and then used Savitzky-Golay filter to deal with noisy signal for each curve. Finally, a long-term change trend (*EVItr*) for each pixel is extracted.

Secondly, we computed the weight for each point in the 163 samples time-series (W_i) data. The weights will be further used in the iteration of EVI reconstruction. It is supposed that the closer the

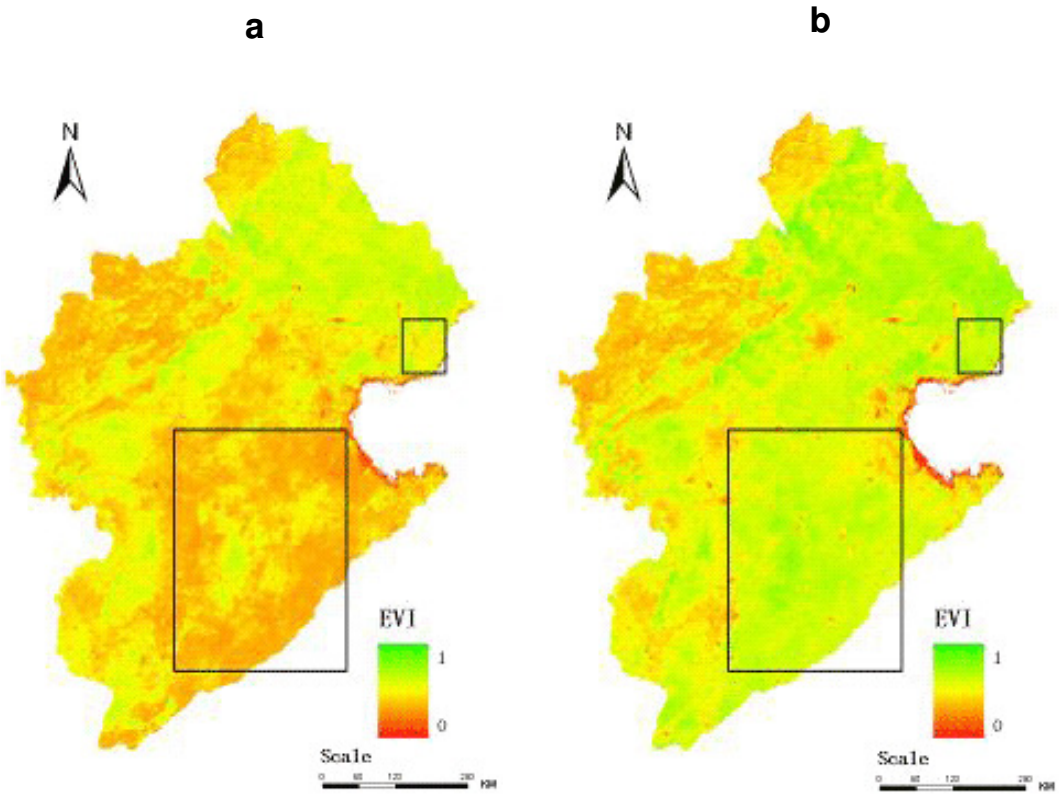

Figure 5. (a) A MODIS EVI image from 26 June to 11 July 2005 and (b) the result of reconstructed dataset.

points to the trend curve, the more likely it reflects the actual vegetation cycle, then the higher the weights we give to the pixel. The weight can be calculated as follows:

$$W_i = \begin{cases} 1 & , \ EVI_i^0 \geq EVI_i^{tr} \\ 1 - d_i / d_{\max} & , \ EVI_i^0 < EVI_i^{tr} \end{cases} \quad (4)$$

Where i ranges from 1 to 163, EVI_i^0 is the value of EVI0 of ith point, EVI_i^{tr} is the value of *EVItr* of the ith point, d_i is the absolute distance from EVI_i^0 to EVI_i^{tr}, d_{max} is the maximum of d_i.

The third step is to refit the EVI time-series on the basis of assumption (2). If EVI_i^0 is less than EVI_i^{tr} for each point in the163 samples, it will be simply replaced by EVI_i^{tr}. And we named this newly generated EVI time-series as *EVI1*.

Fourthly, using the Savitzky-Golay filtering to smoothing the time-series *EVI1* which is same as first step, and refitting the smoothed curves using the method mentioned in the third step, a new EVI time-series is generated which was named *EVI2*.

Fifthly, the processes in fourth step are iterating until the ending condition is satisfied. And a new EVI time-series (EVI_k) is generated, where EVI_k is the kth result of new EVI time-series data.

Finally, the iteration will end when the following condition is satisfied, and the high quality EVI time-series data is generated.

$$F_k = \sum_{i=1}^{163} (| EVI_i^{k+1} - EVI_i^0 | \times W_i)$$
$$F_{k-1} \leq F_k \leq F_{k+1} \quad (5)$$

Parallel computing for the implementing of the algorithm with IDL

As the image data volume is huge, for instance, one image of Haihe River Basin consists of 656×893 pixels with the spatial resolution of 1 *km*1 km*, it is difficult for a normal PC to read the 163 images at a time. In addition, it is time consuming for reading images. Considering the underlying parallelism of the algorithm, we took a parallel strategy and decomposed the spatial data. The parallel strategy involves four steps, which are spatial data decomposition, calculation in parts, mosaic of sub-result and output. The parallel strategy reduces the time for processing to less than 20 h, and it is absolutely necessary especially for dealing with larger images.

RESULTS AND ANALYSIS

Spatial comparison of the reconstructed EVI and MOD13A2-EVI

Figure 5 lists an example of results before and after time-series reconstruction of the MODIS EVI in Haihe River

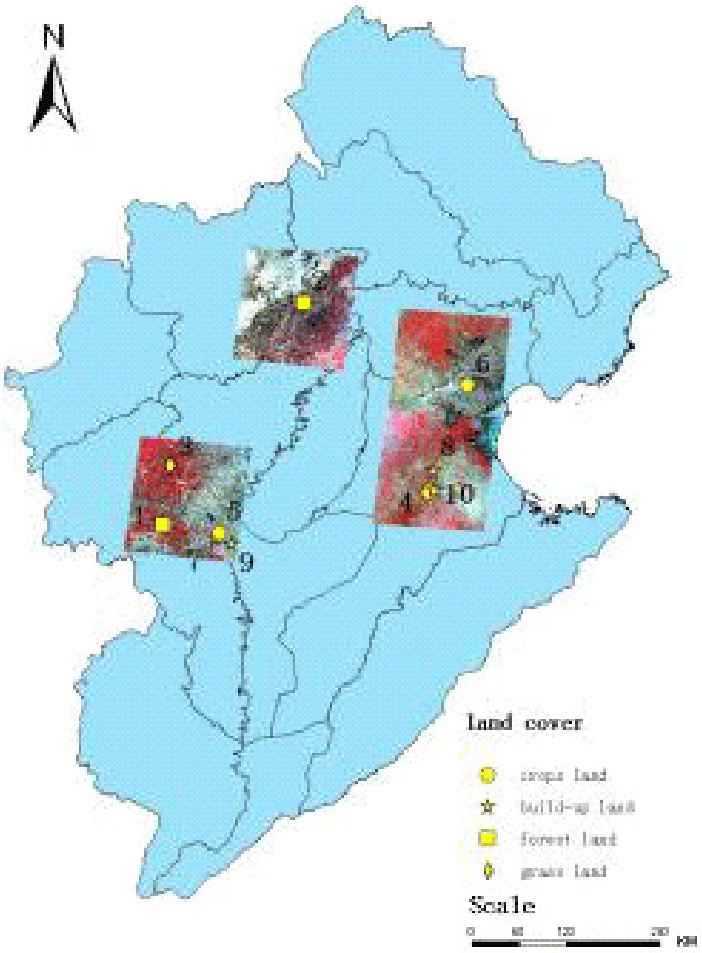

Figure 6. Location of CBERS images and samples.

Basin. The 16 day composite image is from 26 June to 11 July 2005, which is the period for vegetation growth. As shown in Figure 5a, there is a wide range of low–value region in the southern of the original image, which indicates that a large part of this area is city or water. In fact, most pixels within the rectangles correspond to crops land which will present high-value of EVI as displayed in Figure 5b, where the reconstructed EVI displays a more homogeneous result for actual land-cover type. As shown in Figure 5b, the low EVI values of anomalous pixels are replaced and the image is spatially smoother. It is found out that amongst all the 318,075 available pixels, there are respectively 49,454 pixels in original image and 9,517 pixels in the reconstructed image whose EVI values are less than 0.2. We recognized that such kinds of pixels are not vegetation land between June and July. As illustrated for the threshold of 0.2, the percentage of vegetation land is less than 84.5% in Figure 5a, while it is almost 97% in Figure 5b. Considering the vegetation land area account for 94% out of Haihe River Basin, the reconstructed EVI data set is closer to the truth.

Temporal analysis according to different land-use types

Here, a time-series analysis of reconstructed EVI at pixel level was carried out for different land-use types. To get the details of the EVI time-series, all data in the whole year of 2005 were applied. The land-use map is extracted from the China and Brazil earth resource satellite (CBERS) images by the aid of the land-use map of China of the scale 1:250,000 in 2000. Both of the data are provided by the Resources and Environmental Sciences Data Center of Chinese Academy of Sciences. Figure 6 shows the 10 testing pixels and their locations of CBERS images. Table 1 shows the information of the ten samples. Figure 7 shows the details of part of sample points in CBERS image which is false-colour composited with three bands of 4, 3 and 2.

The 10 sample pixels, which are chosen randomly in spatial in Haihe River Basin, include four typical land-use types which are forest, grass land, cropland and built-up land. The samples of 4, 5 and 6 represent two planting patterns in Haihe River Basin. That is, in pixel 4, winter

Table 1. The information of samples.

Sample	Land-use type	Date of images
1	Forest land	15-6-2005
2	Forest land	27-4-2005
3	Grass land	15-6-2005
4	Cropland	20-7-2005
5	Cropland	15-6-2005
6	Cropland	3-5-2005
7	Built-up land	15-6-2005
8	Built-up land	20-7-2005
9	Built-up land	15-6-2005
10	Built-up land	20-7-2005

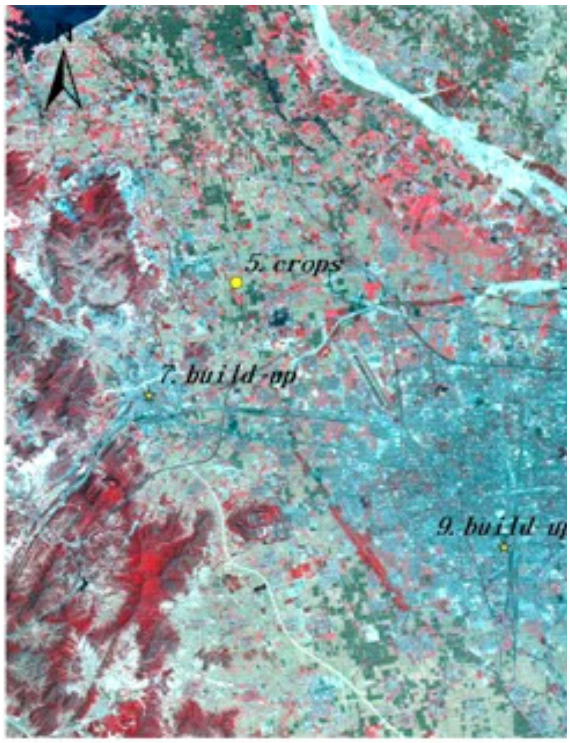

Figure 7. Details of part of the sample points in CBERS.

wheat is full flourish from April to May and harvested in June. After May, summer corn is planted and harvested by the end of September. Different from pixel 4, in pixel 5 and 6, only corn is planted.

To each testing pixels, we extracted 23 values in 2005 before and after reconstruction. Figure 8 lists the patterns of EVI time-series in 2005 of the 10 testing pixels. It is significant that to all the sample pixels, the new EVI data made a smoother time-series profile. This further improves the temporal homogeneousness of EVI. Figures 8a to c illustrated the effect of reconstruction in the vegetation types of forest and grass land. To the forest and grass land, the EVI time-series gets one crest in the middle of a year, that is, August. August is the time when vegetation flourishes. The reconstructed EVI time-series is smoother and the abnormally low or high values in original images can be considered as poor quality pixels and eliminated. The new time-series is closer to the real life condition, that is, it fits to natural rules of vegetation growth. Figures 8d to f describes the EVI time-series patterns of the three crops land pixels. In Figure 8d, the new EVI time-series is very different from the original one. The original one is desultory and contains three troughs which are not conforming to the characteristics of the crops growth. As mentioned previously, two crops of winter wheat and summer corn

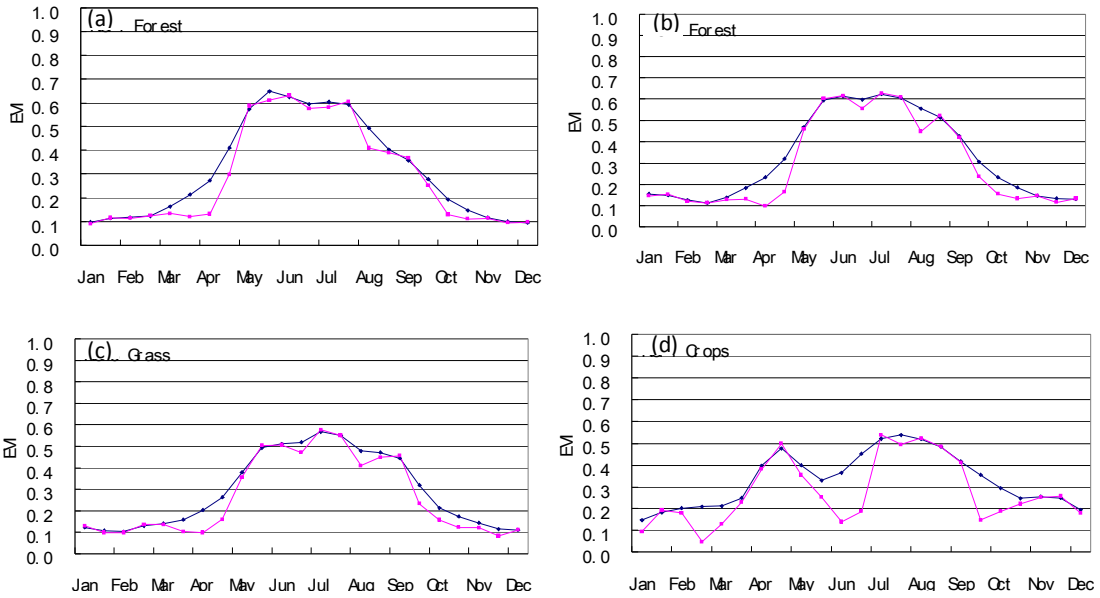

Figure 8. Comparison of original and reconstructed MOD13A2-EVI time-series.

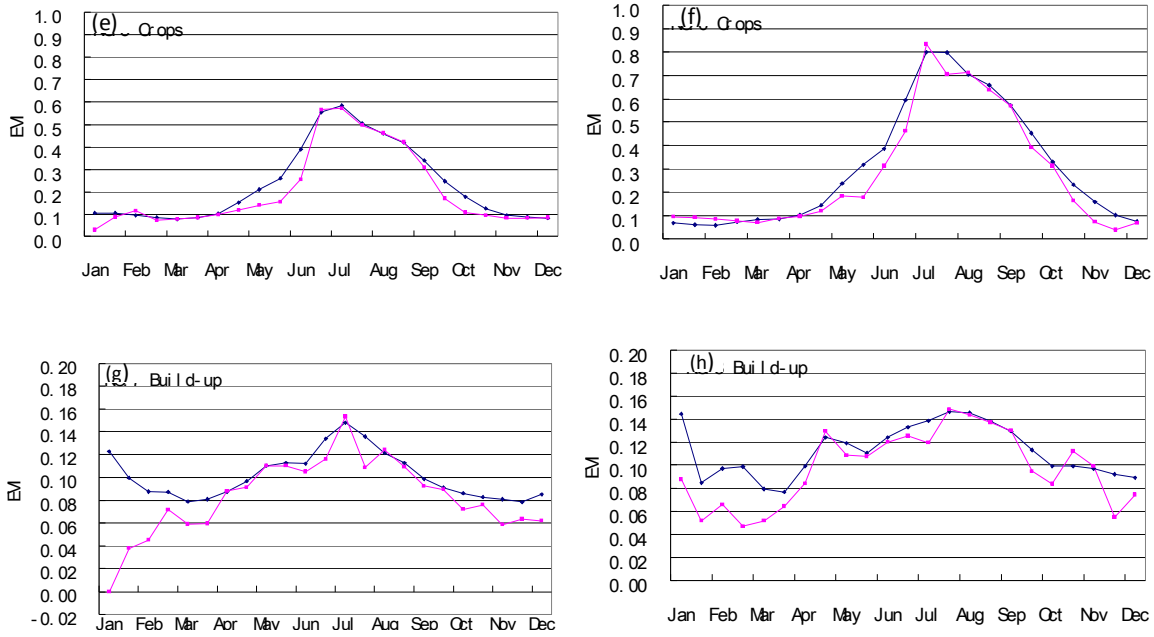

Figure 8. Contd.

are rotationally grown in this area, the EVI profile will appear two peaks and one trough between them. The new time-series displays a good double-peak pattern which can be used to identify the land-use pattern reversely, that is, the annually double-cropping land. The patterns of crops land pixels shown in Figures 8e and f are similar. This is not surprising to us, as they are composed by grass land and forest land. It is noted that two pixels representing the land-use of annually one-cropping land are consistent with the crop type of the location. Compared with the patterns of grass land and forest land, the peaks of the crop land profiles are much narrower. One of the possible reasons is that the period of the harvest is short and it makes the EVI value drop rapidly. Figures from 8.7 to 8.10 illustrate the results of the reconstruction of built-up land. Compared with other vegetation land-use types, the EVI values of the built-up land are lower and the time-series profiles are more

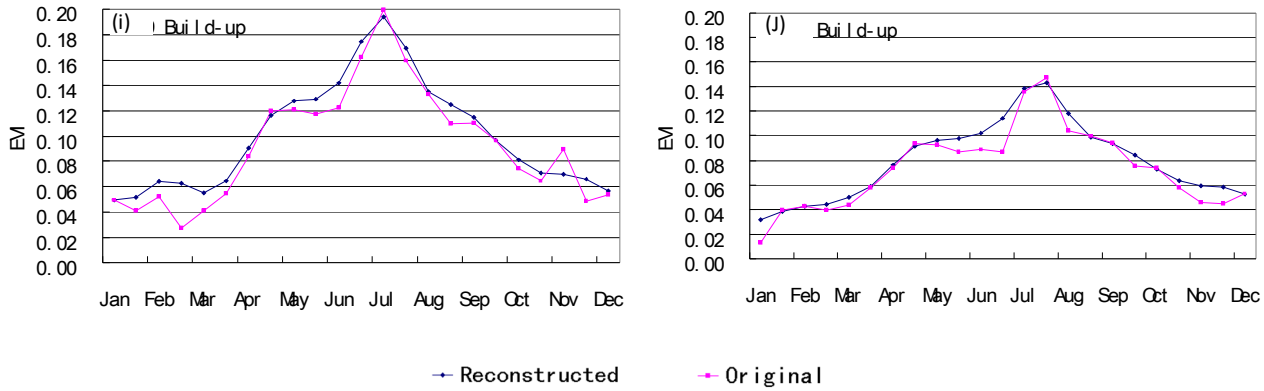

Figure 8. Contd.

zigzag. One of the possible reasons for the low value of EVI is that, built-up land is barren for vegetation, only some sparse greenbelt can be found in big city. Besides, some man-made factors also affect EVI values. Comparing to the four figures, Figures 8g and h are distinguished from Figures 8i and j. The new time-series of Figures 8g and h are obviously higher than original one in winter. After checking CBERS images and land-use map, we find that the seventh and eighth pixels are both small rural built-up land, while the ninth and tenth pixels are both located in city. Around the small built-up land in rural, there is large area of crops-land. This land use pattern will increase the EVI values of the poor quality pixels when we carried out spatial interpolation introduced in spatial interpolation of poor quality pixels. There is a lot of rural built-up land scattering in crops land in Haihe River Basin, so some EVI values of these places will be increased after reconstruction. So these values are untrue.

Conclusion

High-quality VI time-series is an important parameter for crop monitoring and yield estimation. Significant residual noises primarily caused by cloud contamination and atmospheric variability greatly constrain its further application. In this study, we focused on reconstructing MOD13A2-EVI time-series data. Taking Haihe River Basin in North China as an example, we illustrated how to reconstruct the dataset on the basis of Savitzky–Golay filter model.

It is found out that the reconstructed EVI data are more homogeneous and smoother after eliminating values of anomalous pixels spatially; and in vegetation area such as grass land, forest land and crops land, the proposed EVI time-series is closer to real life condition temporally. From the aspect of time-series, it is easy for us to detect the growth, fading or harvest periods. Our further research will focus on how to improve the accuracy of some small dirty built-up land by the filter model.

ACKNOWLEDGEMENTS

This research was supported and funded by Chinese Academy of Sciences (grant KZCX2-YW-310), the Ministry of Science and Technology of China (grant 2008BAK50B01-3) and National Natural Sciences Funds of China (grant 40921140410).

REFERENCES

Zhao YS (2003). The Application Principle and Method of Remote Sensing. Science Press: Beijing, pp. 366-399.
Justice CO, Townshend JRG, Holben BN, Tucker CJ (1985). Analysis of the phenology of global vegetation using meteorological satellite data. Int. J. Remote Sens., 6(8): 1271-1318.
Toshihiro S, Masayuki Y, Hitoshi T, Hitoshi T, Michio S, Naoki I, Hiroyuki O (2005). A crop phenology detection method using time-series MODIS data. Rem. Sens. Environ., 96: 366-374.
Unganai LS, Kogan FN (1998). Drought monitoring and corn yield estimation in southern Africa from AVHRR data. Remote Sens. Environ., 63(3): 219-232.
Running SW, Nemani RR (1988). Relating seasonal patterns of the AVHRR vegetation index to simulated photosynthesis and transpiration of forests in different climates. Rem. Sens. Environ., 24: 347-367.
Tucker CJ, Townshend JRG, Goff TE (1985). African land cover classification using satellite data. Science, 227(4685): 369-375.
Chen J, Per J, Masayuki T, Gu ZH, Bunkei M, Lars E (2004). A Simple Method for Reconstructing a High-quality NDVI Time-series Data Set Based on the Savitzky-Golay Filter. Rem. Sens. Environ., 91: 332-344.
Ma MG, Frank V (2006). Reconstructing pathfinder AVHRR land NDVI time-series data for the Northwest of China. Adv. Space Res., 36: 835-840.
Viovy N, Arino O, Belward AS (1992).The Best Index Slope Extraction (BISE): A method for reducing noise in NDVI time-series. Int. J. Remote Sens., 13(8): 1585-1590.
Huete A, Justice C, Van LW (1999). MODIS vegetation index (MOD13) algorithm theoretical basis document. http://modis.gsfc.nasa.gov/data/atbd/atbd_mod13.pdf.
Lovell JL, Graetz RD (2001). Filtering pathfinder AVHRR land NDVI data for Australia. Int. J. Remote Sens., 22(13): 2649-2654.

Cihlar J (1996). Identification of contaminated pixels in AVHRR composite images for studies of land biosphere. Rem. Sens. Environ., 56: 149-153.
Cihlar J, Ly H, Li ZQ, Chen J, Pokrant H, Huang FT (1997). Multitemporal, multichannel AVHRR data sets for land biosphere studies—artifacts and corrections. Rem. Sens. Environ., 60: 35-57.
Swets DL, Reed BC, Rowland JD, Marko SE (1999). A weighted leasts-quares approach to temporal NDVI smoothing. Pro of the American Society of Photogrammetric Remote Sensing (ASPRS), Washington DC, USA, pp. 526-536.
Jose E, Ryutaro T, Renchin T (2002).The polynomial least squares operation (PoLeS): a method for reducing noise in NDVI time series data. http://www.gisdevelopment.net/aars/acrs/2002/index.htm
Chappell A, Seaquist JW, Eklundh L (2001).Improving the estimation of noise from NOAA AVHRR NDVI for Africa using geostatistics. Int. J. Remote Sens., 22(6): 1067-1080.
Jonsson P, Eklundh L (2002). Seasonality extraction by function fitting to time-series of satellite sensor data. IEEE Trans. Geosci. Rem. Sens., 40(8): 1824-1832.
Savitzky A, Golay MJE (1964). Smoothing and Differentiation of Data by Simplified Least Squares Procedures. Anal. Chem., 36: 1627-1639.
http://modis.gsfc.nasa.gov/index.php